

Comparative study of the luminescence and intrinsic point defects in the kesterite $\text{Cu}_2\text{ZnSnS}_4$ and chalcopyrite $\text{Cu}(\text{In,Ga})\text{Se}_2$ thin films used in photovoltaic applications

Manuel J. Romero,* Hui Du, Glenn Teeter, Yanfa Yan, and Mowafak M. Al-Jassim

National Renewable Energy Laboratory (NREL), 1617 Cole Boulevard, Golden, Colorado 80401-3393, USA

(Received 29 April 2011; revised manuscript received 4 August 2011; published 24 October 2011)

The kesterite $\text{Cu}_2\text{ZnSnS}_4$ (CZTS) is attracting considerable interest because first-principles calculations predict that its electronic properties must be similar to their associated chalcopyrite $\text{Cu}(\text{In,Ga})\text{Se}_2$ (CIGS) compounds [Chen *et al.*, *Phys. Rev. B* **81**, 245204 (2010)]. Here, the authors report on first experimental evidence of the close resemblance in the luminescence of Cu-poor kesterites and Cu-poor chalcopyrites used in photovoltaic applications. Microluminescence measurements suggest that even the very distinct electronic structure of grain boundaries in CIGS is present, to some extent, in CZTS. The similarities between CIGS and CZTS become more pronounced as the efficiency of the CZTS solar cells gradually increases. The implications of these results for the future development of CZTS solar cells are discussed.

DOI: [10.1103/PhysRevB.84.165324](https://doi.org/10.1103/PhysRevB.84.165324)

PACS number(s): 78.55.Et, 61.72.Mm, 78.60.Hk, 84.60.Jt

I. INTRODUCTION

$\text{Cu}(\text{In,Ga})\text{Se}_2$ (CIGS) has recently demonstrated a record efficiency of 20.0%, the absolute record for all thin-film photovoltaics (PVs).¹ Although CIGS is at present positioned to compete in the solar energy business at a production capacity approaching one gigawatt, these compounds cannot possibly meet the projected demand for solar energy because of the relative scarcity of indium and the competition for this resource with other manufacturing sectors.^{2,3} In this regard, the kesterite $\text{Cu}_2\text{ZnSnS}_4$ (CZTS) is attracting considerable interest because it contains all abundant elements Cu, Zn, Sn, and S, and the reported bandgap is near the optimum for PV applications. First-principles calculations predict that our understanding of the electronic structure and defect formation in the chalcopyrite structure of CIGS can be partly extrapolated to CZTS in the kesterite structure.^{4,5} CZTS, on the other hand, shows a very limited region of stability in the Cu_2S - ZnS - SnS_2 phase diagram, and minor deviations from stoichiometry leads to the formation of secondary phases such ZnS , CuS , Cu_2S , and SnS_2 .^{4,6} The demonstration of CZTS thin films with the required electronic properties and free of these binaries is of the highest priority for the potential development of solar cells based on these compounds.

The success of CIGS is based primarily on the benign character of its electronic structure, which, in the regime of Cu deficiency, is dominated by the formation of copper vacancies (V_{Cu}) and the stabilization of defect complexes with low formation energies such $(2V_{\text{Cu}}^- + \text{In}_{\text{Cu}}^{2+})$.^{7,8} Under these conditions, grain boundaries develop a distinct electronic structure that, because of its benign character as well,⁹ is absolutely critical to achieving high efficiency in CIGS solar cells. These beneficial effects can be measured by luminescence spectrum imaging,¹⁰ which provides a direct correlation between the microstructure of the CIGS and the electronic properties as revealed on the emission spectrum. The obvious question is whether similar electronic effects are present in the kesterite structure of CZTS. In this contribution, luminescence spectroscopy and spectrum imaging measurements are applied to CZTS, and the results are compared with the high-efficiency CIGS obtained by the three-stage process. The implications of

these results for the future development of CZTS solar cells will be further discussed.

CZTS thin films are obtained by coevaporation of Cu, Zn, and Sn from three independent effusion cells under a molecular beam of S_2 supplied by a valved-cracking source. The molybdenum-coated glass substrates are actively heated to 470 °C. The base pressure of the chamber is 8.0×10^{-6} Torr, rising to 1.7×10^{-4} Torr during deposition. More details, including information on the elemental sources, can be found in Ref. 6. The stoichiometry of the films used in this study is confined to the region of stability for the kesterite phase and slightly displaced toward the ZnS - SnS_2 boundary of the phase diagram. These CZTS films are therefore Cu-poor [$\text{Cu}/(\text{Zn} + \text{Sn}) \sim 0.74$] and Zn-rich ($\text{Zn}/\text{Sn} \sim 1.36$), which is consistent with the stoichiometry of the best CZTS solar cells reported in the literature.^{11,12} The $\text{Cu}/(\text{In} + \text{Ga})$ ratio for our reference CIGS is ~ 0.9 , and $\text{Ga}/(\text{In} + \text{Ga}) \sim 0.3$, as required for record performance.¹³

II. LUMINESCENCE SPECTROSCOPY

The fundamental aspects of recombination in Cu-poor kesterites are first investigated by luminescence spectroscopy, and the results are compared with those previously obtained in Cu-poor chalcopyrites. The influence of the excitation density (measured by the electron-beam current I_b)¹⁴ on the emission spectrum at cryogenic temperatures ($T = 15$ K) is shown in Figs. 1(a) and 1(b) for CIGS and CZTS, respectively. These measurements are complemented with the influence of the temperature [$\Delta T = 20$ – 300 K; Figs. 1(c) and 1(d)]. We observe extraordinary similarities between these Cu-poor thin films. In both CIGS and CZTS, the spectrum consists of a broadband luminescence centered a few hundreds of millielectronvolts (meV) below the bandgap E_g . The emission spectrum shows a pronounced *blueshift* with excitation density (about 50 meV for CIGS over three decades and about 50 meV for CZTS over four decades) and a blueshift with temperature.

The luminescence of Cu-poor CIGS has been extensively investigated by other authors,^{15,16} and here, we summarize the aspects most relevant to our comparative study of chalcopyrites and kesterites. This is better described by considering first the

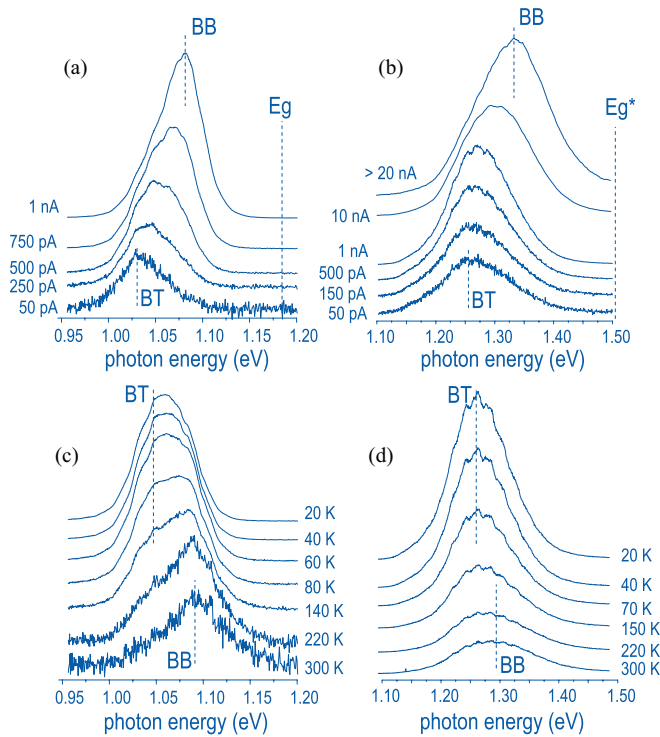


FIG. 1. (Color online) Influence of the excitation density (measured by the electron beam current I_b) on the emission spectrum of (a) Cu-poor CIGS and (b) Cu-poor, Zn-rich CZTS at cryogenic temperatures ($T = 15$ K). Influence of the temperature ($T = 20$ – 300 K) of the emission spectrum of CIGS at $I_b = 500$ pA and of CZTS at $I_b = 1$ nA, panels (c) and (d) respectively.

point defect structure of chalcopyrites under Cu deficiency. From first-principles calculations,¹⁷ the dominant donors and acceptors are, respectively, the indium-on-copper-antisite (In_{Cu}) (stabilized through the formation of $(2V_{\text{Cu}}^- + \text{In}_{\text{Cu}}^{2+})$ defect complexes) and the copper vacancy (V_{Cu}). The prevalence of these intrinsic point defects in the chalcopyrite structure leads to delocalization of the donor and acceptor states and the formation of bands. In this scenario of a high density of intrinsic point defects and compensation, local deviations in the distribution of donors (+) and acceptors (–) will introduce potential fluctuations in the band structure.¹⁸ The schematics of the band diagram (including these potential fluctuations) are shown in Fig. 2. Using this representation, the luminescence includes two emission bands: one associated with the band tails of the donor and acceptor bands (BT)—which follow the potential fluctuations—and the other to transitions between the donor and acceptor bands (BB),¹⁶ as shown schematically in Fig. 2. At low temperature and low excitation density [$I_b = 50$ pA in Fig. 1(a)], the spectrum is dominated by band-tail transitions corresponding to the lowest energy states in the landscape of potential fluctuations. The blueshift with the excitation density at low temperature results from the reduction of the amplitude of the potential fluctuations, leading to an increase in the transition energy [toward BB, $I_b = 1$ nA in Fig. 1(a)]. In our case, we observe a saturation of the transition energy at high excitation densities ($I_b > 1$ nA) below the measured bandgap.¹⁹ This suggests that (quasi-)free electron to acceptor band transitions are

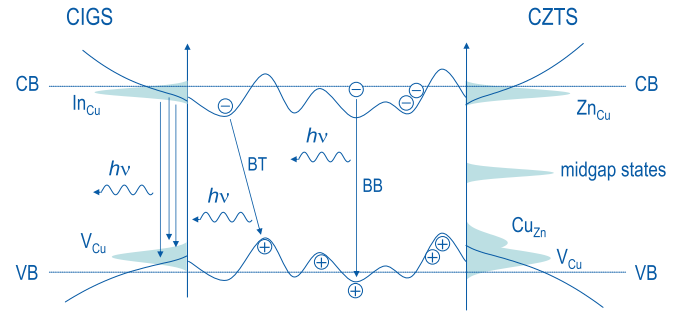


FIG. 2. (Color online) Schematics of the band diagram for Cu-poor CIGS and Cu-poor, Zn-rich CZTS. The luminescence is dominated by band-tail (BT) and band-to-band (BB) transitions between delocalized donor and acceptor states. Local deviations in the distribution of donors and acceptors lead to potential fluctuations.

dominant at high excitation densities ($\Delta n, p > 10^{17}$ cm^{-3}) with no contribution of the excitonic transitions observed in near stoichiometric chalcopyrites.²⁰ The overall blueshift with temperature [Fig. 1(c)] is a direct consequence of the thermal excitation of electrons (holes) from the band-tail states to the donor (acceptor) band, resulting in the quenching of the BT transition observed at moderate excitation densities [$I_b = 500$ pA; Fig. 1(c)] and the increase in the energy of free electrons (holes) in the donor (acceptor) bands with further increasing temperature, resulting in the blueshift of the BB transition.

Similar spectroscopy measurements in Cu-poor kesterites reveal a near one-to-one correspondence with Cu-poor chalcopyrites [Figs. 1(a)–1(d)]. The spectrum also consists of BT and BB emission bands with similar excitation density and temperature dependencies to those observed in chalcopyrites. The most prominent difference is the exceedingly high excitation density ($I_b > 10$ nA, $\Delta n, p > 10^{18}$ cm^{-3}) needed to transition from a band-tail to a band-to-band recombination in the kesterite [Fig. 1(b)]. Saturation of the transition energy is observed at $I_b > 20$ nA. This is accompanied by a much lower efficiency of the photon emission (a factor of 1/50). Interestingly, among the surprising similarities, the saturation of the transition energy does happen at about 150–200 meV below the bandgap in both CIGS and CZTS. The overall blueshift, with temperature seen at $I_b = 1$ nA [Fig. 1(d)], is a direct consequence of the thermal excitation of the band-tail states, as observed for CIGS [Fig. 1(c)] at $I_b \ll 1$ nA. In summary, there is a near one-to-one correspondence if we factor in for the higher excitation needed to observe similar effects in kesterites.

These results point to a similar scenario of a high density of intrinsic point defects and compensation for Cu-poor kesterites, leading to the introduction of potential fluctuations in the band structure (see Fig. 2). From first-principles calculations,⁵ the copper-on-zinc antisite (Cu_{Zn}) is the dominant intrinsic point defect in CZTS with the lowest formation energy and an acceptor level at $\varepsilon(-/0) = 0.12$ eV. The V_{Cu} -acceptor state, with a shallow level at $\varepsilon(-/0) = 0.02$ eV (similar to that of CIGS at $\varepsilon(-/0) = 0.03$ eV), follows after Cu_{Zn} . The dominant donor corresponds to the zinc-on-copper antisite (Zn_{Cu}) (stabilized through the formation of $(\text{Cu}_{\text{Zn}}^- + \text{Zn}_{\text{Cu}}^+)$ defect complexes). When we consider that the best kesterite

thin films are obtained under Cu-poor, Zn-rich conditions, promoting the formation of V_{Cu} and suppressing the formation of Cu_{Zn} (like those used here), the resulting band diagram for the CZTS looks very much like that of CIGS (see Fig. 2).

However, the larger number of possible intrinsic point defects in CZTS from antisite substitutions among the cations Cu(I), Zn(II), and Sn(IV) can lead to increased recombination. Of those with low formation energy (Cu_{Zn} , Cu_{Sn} , Zn_{Sn} , and the vacancies V_{Cu} and V_{Zn}), Cu_{Sn} is potentially very detrimental to efficiency, with a transition energy level close to the midgap.⁵ In addition to Cu_{Sn} , other substitutional defects of the multivalent element Sn (Sn_{Cu} ²¹ and Sn_{Zn}) result in electronic transitions deep inside the bandgap.

The relatively low intensity of the luminescence emitted from CZTS is a direct consequence of the nonradiative recombination associated with these defects. The higher excitation ($I_b = 10$ nA vs $I_b = 1$ nA) needed to transition from a spectrum dominated by band-tail recombination and potential fluctuations to band-to-band recombination is also consistent with the competing radiative and nonradiative recombination processes, effectively bringing down the electron (hole) densities populating the donor (acceptor) bands. As a consequence, high injection conditions are only achieved at very high excitation densities ($I_b > 20$ nA). The spectrum is then dominated by transitions involving free electrons in the conduction band and holes in the acceptor band. The observation that the transition energy (relative to the bandgap) is similar for kesterites and chalcopyrites suggests that the Cu vacancy is the dominant acceptor in both. For CZTS, this is observed under Cu-poor, Zn-rich conditions, promoting the formation of V_{Cu} and suppressing the formation of Cu_{Zn} . The transition energy at saturation moves into the bandgap when Cu_{Zn} is expected to be the dominant acceptor in the kesterite.

III. LUMINESCENCE FROM GRAIN BOUNDARIES

One exceptional aspect of the electronic properties in chalcopyrites, and one critical to the success in photovoltaic applications, is the benign behavior of grain boundaries. The leading explanation for this behavior assimilates the interface of the grain boundary to the $\{112\}$ -oriented polar free surfaces of the CIGS, which are stabilized by the formation of V_{Cu} . The predicted valence band offset caused by the removal of copper atoms from the boundary leads to the formation of a neutral barrier for holes that do not otherwise impede the electron transport and reduce recombination.²² The existence of this neutral barrier has been confirmed experimentally by several methods.^{10,23–25} In our case, microluminescence measurements based on spectrum imaging revealed a redshift of the emission spectrum at grain boundaries. Figure 3(a) shows a map of the photon energy of the luminescence from CIGS (color coded so that red and blueshifts in the emission spectrum are intuitive²⁶). Figure 3(b) is equivalent to Fig. 3(a) but with higher contrast. We observe a 10–15 meV redshift of the luminescence at grain boundaries when compared with the grain interiors. This is consistent with the copper depletion observed at grain boundaries by atom probe tomography:²⁷ the incorporation of V_{Cu} acceptor states will extend the acceptor band into the gap, hence the observed redshift. We have firmly established that this redshift is absolutely critical in achieving

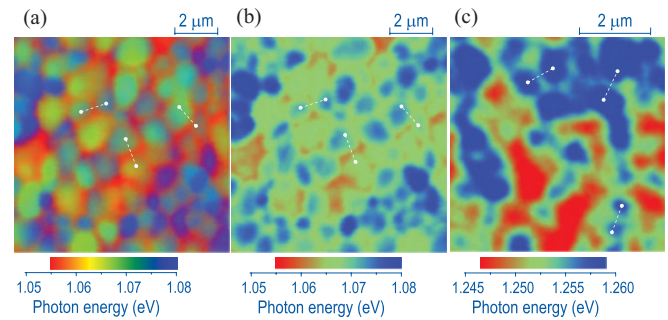


FIG. 3. (Color) Microluminescence measurements. (a) A representative map of the photon energy of the luminescence from CIGS thin films used in PV applications. A redshift of the emission spectrum (10–15 meV) is observed at grain boundaries. (b) Another version of the photon energy map with a basic color scale. This scale is needed to increase the contrast so (c) the less significant redshifts (4–5 meV) in the emission spectrum of grain boundaries in CZTS are visible.

high efficiency in CIGS and must be related to the formation of the neutral barrier.

Is the electronic structure of grain boundaries in kesterites and chalcopyrites related? Figure 3(c) shows a map of the photon energy of the luminescence from CZTS which indeed shows this redshift of the emission spectrum for a number of grain boundaries. The redshift is less pronounced for the kesterites (4–5 meV in CZTS vs 10–15 meV in CIGS), suggesting less differentiation in the distribution of intrinsic point defects at the grain boundary, a probable consequence of the higher degree of cation disorder in the kesterite structure. The photon energy map of Fig. 3(c) also reveals that differences in the electronic structure within the grain interiors in CZTS are often more significant than the redshift at grain boundaries. This is very different from CIGS [Figs. 3(a) and 3(b)], whose redshift at the grain boundaries is the most dominant effect and variations from grain to grain are minimal. The increased disorder of the kesterite structure might be once again responsible for this effect.

IV. ELECTRONIC PROPERTIES AND EFFICIENCY

The results reported in the previous sections correspond to the best co-evaporated CZTS thin films at the current stage of development at NREL. This final section covers the correspondence between electronic properties of the CZTS thin film and efficiency of the solar cell. We have observed that the similarities between CIGS and CZTS become more pronounced as the efficiency of the CZTS solar cells gradually increases. Figure 4 shows the results of the luminescence spectroscopy measurements for CZTS solar cells of increasing efficiency and the CIGS reference cell: K^0 (0.0%) < K^1 (1.8%) < K^2 (2.3%) < C (18.7%), with K for kesterite and C for chalcopyrite. In the absence of a measurable efficiency (K^0 in Fig. 4), the broadband luminescence extends far into the infrared, suggesting the contribution of deeper transition energy levels such as the Cu_{Zn} acceptor state. Surprisingly, the spectrum is practically insensitive to the conditions of the measurement (I_b and temperature), as shown for I_b in Fig. 4(b). This is likely to be related to the extremely high densities

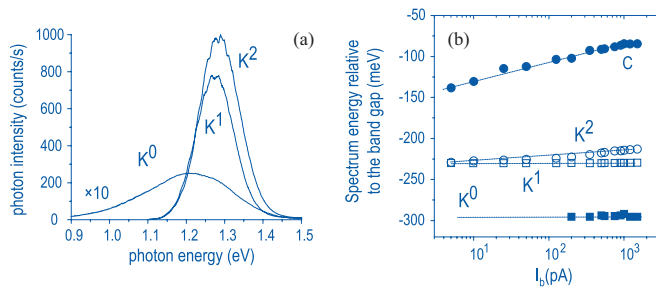


FIG. 4. (Color online) (a) Evolution of the spectrum with increasing efficiency of CZTS solar cells ($K^0 < K^1 < K^2$, with K for kesterite). (b) Influence of the excitation density (measured by the electron beam current I_b) on the energy of the spectrum, relative to the bandgap energy, for K^0 , K^1 , and K^2 and the CIGS reference cell (with C for chalcopyrite).

of intrinsic point defects and compensation suggested by electrical measurements. The demonstration of a measurable photovoltaic effect in the CZTS is accompanied by an abrupt shift of the luminescence toward the bandgap energy [K^1 and K^2 in Fig. 4(a)], which is related to the V_{Cu} becoming the dominant acceptor in CZTS (and the suppression of Cu_{Zn}). This inversion in the population of acceptor states replaces the deep Cu_{Zn} acceptors in CZTS by the shallow V_{Cu} acceptors that dominate the electronic properties of Cu-poor CIGS. As a consequence of this change in the point defect chemistry of the kesterite, K^1 and K^2 begin to show the blueshift with I_b and the blueshift with temperature that is common to Cu-poor CIGS. In CZTS, the sensitivity of the luminescence to the excitation density increases with efficiency ($K^2 > K^1$) as a result of the reduction of near midgap states. From the microluminescence measurements, we observe the first evidence of a redshift at grain boundaries in K^1 with a larger number of grain boundaries showing this behavior in K^2 [as shown in Fig. 3(c)]. In contrast, nearly all grain boundaries in CIGS present the neutral barrier associated with the redshift of the emission spectrum.

These results suggest that a more strict control over the point defect chemistry is absolutely critical to continue improving the efficiencies of kesterite solar cells. We propose surveying the region of stability (or near stability) for the kesterite phase along the phase diagram to find the region where the point defect chemistry (from luminescence spectroscopy or other related measurements) is most similar to the chalcopyrite related phase. Special attention should be given to the suppression of those point defects with associated midgap

states. Luminescence microscopy, in combination with other measurements with micro- and nano-scale resolution, should be applied to investigate the factors responsible for the redshift of the luminescence at grain boundaries in CZTS and the potential for a large neutral barrier. At this stage of development, a limited number of grain boundaries show this behavior, hindering further improvement in efficiency. Coming up with a strategy to bring the neutral barrier to most grain boundaries should be a first priority in the development of CZTS solar cells.

V. SUMMARY AND CONCLUSIONS

We have found that the luminescence properties of Cu-poor kesterites are fundamentally similar to those previously observed in their Cu-poor chalcopyrite relatives: This is a consequence of the close resemblance in the intrinsic point defect structure of CIGS and CZTS, which is characterized by high densities of donor and acceptor states (associated to point defects with low formation energy), leading to high compensation and potential fluctuations. The spectrum is dominated by band-tail recombination at low temperature and low excitation densities and band-to-band transitions when increasing the temperature or the excitation density. The main difference arises from the susceptibility of the kesterite to form point defects with associated electronic states near the midgap, resulting in more nonradiative recombination. This is confirmed not only by the decrease in the intensity of the luminescence, but also by the extremely high excitation densities needed to transition from a BT to BB recombination and then reach high injection conditions. Similar transition energy at saturation (relative to the bandgap) suggests that the copper vacancy is the dominant acceptor in both Cu-poor CIGS and Cu-poor, Zn-rich CZTS. The similarities extend to the electronic structure of grain boundaries: the redshift in the luminescence from grain boundaries in CIGS, which is related to the formation of a large neutral barrier and reduced recombination, is present to some extent in CZTS. The similarities between CIGS and CZTS become more pronounced as the efficiency of the CZTS solar cells gradually increases, suggesting that our fundamental understanding of chalcopyrites supports the development of kesterite solar cells.

ACKNOWLEDGMENT

This work was supported by the US Department of Energy under Contract No. DE-AC36-08-GO28308.

*manuel.romero@nrel.gov

¹P. Jackson, D. Hariskos, E. Lotter, S. Paetel, R. Wuerz, R. Menner, W. Wischmann, and M. Powalla, *Progress in Photovoltaics: Research and Applications* **19**, 894 (2011).

²B. A. Andersson, *Progress in Photovoltaics: Research and Applications* **8**, 61 (2000).

³A. Feltrin and A. Freundlich, *Renewable Energy* **33**, 180 (2008).

⁴A. Nagoya, R. Asahi, R. Wahl, and G. Kresse, *Phys. Rev. B* **81**, 113202 (2010).

⁵S. Chen, J.-H. Yang, X. G. Gong, A. Walsh, and S.-H. Wei, *Phys. Rev. B* **81**, 245204 (2010).

⁶G. Teeter, H. Du, J. E. Leisch, M. Young, F. Yan, S. W. Johnston, P. Dippo, D. Kuciauskas, M. J. Romero, P. Newhouse, S. E. Asher, and D. S. Ginley, in *Proceedings of the 35th IEEE Photovoltaic Specialists Conference (PVSC '10), Honolulu, HI, June 20–25 (2010)*.

- ⁷S. B. Zhang, S.-H. Wei, and A. Zunger, *Phys. Rev. Lett.* **78**, 4059 (1997); S. B. Zhang, S.-H. Wei, A. Zunger, and H. Katayama-Yoshida, *Phys. Rev. B* **57**, 9642 (1998).
- ⁸S.-H. Wei, S. B. Zhang, and A. Zunger, *Appl. Phys. Lett.* **72**, 3199 (1998).
- ⁹Y. Yan, C.-S. Jiang, R. Noufi, Su-Huai Wei, H. R. Moutinho, and M. M. Al-Jassim, *Phys. Rev. Lett.* **99**, 235504 (2007).
- ¹⁰M. J. Romero, K. Ramanathan, M. A. Contreras, M. M. Al-Jassim, R. Noufi, and P. Sheldon, *Appl. Phys. Lett.* **83**, 4770 (2003).
- ¹¹T. K. Todorov, K. B. Reuter, and D. B. Mitzi, *Adv. Mater.* **22**, 1 (2010).
- ¹²K. Wang, O. Gunawan, T. Todorov, B. Shin, S. J. Chey, N. A. Bojarczuk, D. Mitzi, and S. Guha, *Appl. Phys. Lett.* **97**, 143508 (2010).
- ¹³M. A. Contreras, M. J. Romero, and R. Noufi, *Thin Solid Films* **511–512**, 51 (2006).
- ¹⁴As a rule of thumb, an electron beam current of $I_b = 1$ nA corresponds to an excess carrier density of $\Delta n, p \sim 10^{17} \text{ cm}^{-3}$.
- ¹⁵I. Dirnstorfer, M. Wagner, D. M. Hofmann, M. D. Lampert, F. Karg, and B. K. Meyer, *Phys. Status Solidi A* **168**, 163 (1998).
- ¹⁶J. Krustok, H. Collan, M. Yakushev, and K. Hjelt, *Phys. Scr.*, **T 79**, 179 (1999).
- ¹⁷S. H. Wei, S. B. Zhang, and A. Zunger, *Appl. Phys. Lett.* **72**, 3199 (1998); T. Maeda, T. Wada, *J. Phys. Chem. Solids* **66**, 1924 (2005).
- ¹⁸B. I. Shklovskii and A. L. Efros, *Electronic Properties of Doped Semiconductors* (Springer, Berlin, 1984).
- ¹⁹The bandgap is measured by quantum efficiency measurements.
- ²⁰N. Rega, S. Siebentritt, J. Albert, S. Nishiwaki, A. Zajogin, M. Ch. Lux-Steiner, R. Kniese, and M. J. Romero, *Thin Solid Films* **480–481**, 286 (2005).
- ²¹K. Biswas, S. Lany, and A. Zunger, *Appl. Phys. Lett.* **96**, 201902 (2010).
- ²²C. Persson and A. Zunger, *Phys. Rev. Lett.* **91**, 266401 (2003); *Appl. Phys. Lett.* **87**, 211904 (2005).
- ²³C.-S. Jiang, R. Noufi, J. A. AbuShama, K. Ramanathan, H. R. Moutinho, J. Pankow, and M. M. Al-Jassim, *Appl. Phys. Lett.* **84**, 3477 (2004).
- ²⁴M. J. Romero, C.-S. Jiang, R. Noufi, and M. Al-Jassim, *Appl. Phys. Lett.* **87**, 172106 (2005).
- ²⁵M. Hafemeister, S. Siebentritt, J. Albert, M. Ch. Lux-Steiner, and S. Sadewasser, *Phys. Rev. Lett.* **104**, 196602 (2010).
- ²⁶The photon energy map is generated by first defining the region of interest on the emission spectrum (e.g., 0.8–1.1 eV), which is then divided in three different channels (Red, 0.8–0.9 eV; Green: 0.9–1.0 eV; Blue: 1.0–1.1 eV). The total counts in each channel are normalized to the 0–255 scale of the RGB code to generate the color of each pixel.
- ²⁷O. Cojocaru-Miréidin, P.-P. Choi, D. Abou-Ras, and D. Raabe, in *Proceedings of the 37th IEEE Photovoltaic Specialists Conference, Seattle, WA, June 19–24 (2011)*.